Nano Res. 2010, 3(9): 676–684
DOI 10.1007/s12274-010-0031-7
Research Article

ISSN 1998-0124
CN 11-5974/O4

Monodisperse Nickel Nanoparticles Supported on SiO_2 as an Effective Catalyst for the Hydrolysis of Ammonia–Borane

Önder Metin[1,2], Saim Özkar[1], and Shouheng Sun[2] (✉)

[1] Department of Chemistry, Middle East Technical University, 06531, Ankara, Turkey
[2] Department of Chemistry, Brown University, Providence, Rhode Island 02912, USA

Received: 27 June 2010 / Revised: 8 August 2010 / Accepted: 10 August 2010

ABSTRACT

Monodisperse Ni nanoparticles (NPs) have been synthesized by the reduction of nickel(Ⅱ) acetylacetonate with the borane–tributylamine complex in a mixture of oleylamine and oleic acid. These Ni NPs are an active catalyst for the hydrolysis of the ammonia–borane (AB, $H_3N{\cdot}BH_3$) complex under ambient conditions and their activities are dependent on the chemical nature of the oxide support that they were deposited on. Among various oxides (SiO_2, Al_2O_3, and CeO_2) tested, SiO_2 was found to enhance Ni NP catalytic activity due to the etching of the 3.2 nm Ni NPs giving Ni(Ⅱ) ions and the subsequent reduction of Ni(Ⅱ) that led to the formation of 1.6 nm Ni NPs on the SiO_2 surface. The kinetics of the hydrolysis of AB catalyzed by Ni/SiO_2 was shown to be dependent on catalyst and substrate concentration as well as temperature. The Ni/SiO_2 catalyst has a turnover frequency (TOF) of 13.2 mol $H_2{\cdot}$(mol Ni)$^{-1}{\cdot}$min^{-1}—the best ever reported for the hydrolysis of AB using a nickel catalyst, an activation energy of 34 kJ/mol ± 2 kJ/mol and a total turnover number of 15,400 in the hydrolysis of AB. It is a promising candidate to replace noble metals for catalyzing AB hydrolysis and for hydrogen generation under ambient conditions.

KEYWORDS

Nickel nanoparticles, supported catalyst, hydrogen storage, hydrolysis of ammonia–borane

1. Introduction

Controlled storage and release of hydrogen are the key challenges facing the transition to a hydrogen economy. Due to safety concerns and volumetric constraints, conventional high-pressure and cryogenic storage/release systems are impractical for mobile applications [1, 2]. Recently, the ammonia–borane (AB, $H_3N{\cdot}BH_3$) complex was identified as one of the leading candidates for a hydrogen storage material: it has high hydrogen content (19.6 wt%), high stability under ordinary fuel cell operating conditions and nontoxicity [3–6]. The stored hydrogen can be released from AB via a catalytic hydrolysis route [7]. The hydrolysis of AB in the presence of a suitable catalyst yields 3 moles of hydrogen per mole of AB at room temperature, as shown in the following Eq. [8]:

$$H_3N\cdot BH_3(aq) + 2H_2O\ (L) \xrightarrow{\text{catalyst}} (NH_4)BO_2(aq) + 3H_2(g)$$

A number of transition metals or their alloys have been tested as catalysts for the hydrolysis of AB [9–13] and rapid hydrogen generation has been achieved by using the precious metal catalysts Pt, Rh, Ir, and Ru

Address correspondence to ssun@brown.edu

[14–18]. However, for practical use, the development of lower cost catalysts is required. Recently, two types of Ni nanoparticles (NPs) stabilized by starch [19] or poly(*N*-vinyl-2-pyrrolidone) [20] as well as bimetallic Ni–Au NPs [21] have been reported to be promising catalysts for the hydrolysis of AB. In a more recent communication, we demonstrated a facile synthesis of monodisperse 3.2 nm Ni NPs [22]. When these Ni NPs were supported on Ketjen carbon black, they were shown to be a highly active catalyst for the hydrolysis of AB, with the total turnover frequency (TOF) reaching 8.8 mol H_2·(mol Ni)$^{-1}$·min^{-1}. However, the Ni/C catalyst was not stable during the catalytic reaction, losing ~20% of its initial activity after the 5th catalytic run due to the agglomeration of Ni NPs on the carbon support. In the search for a better support material to enhance the stability of these NPs during the catalytic hydrolysis of AB at room temperature, we tested a variety of oxides including SiO_2, Al_2O_3, and CeO_2. We found that 3.2 nm Ni NPs supported on SiO_2 showed the highest activity and durability. Herein we report our detailed studies of the synthesis and characterization of the Ni/SiO_2 catalyst and its catalysis of the hydrolysis of AB.

2. Experimental

2.1 Materials

Oleylamine (OAm, >70%), oleic acid (OA, 90%), nickel(Ⅱ) acetylacetonate (Ni(acac)$_2$, 95%), ammonia–borane (AB) complex (97%), borane–tributylamine complex (BTB), aluminum oxide (Al_2O_3; particle size <50 nm (BET)) and cerium(Ⅳ) oxide nanopowder (CeO_2; particle size <50 nm (BET), >99.95% trace metals basis) were purchased from Sigma–Aldrich®. Neutral silica powder (SiO_2, 60–200 mesh) was purchased from J. T. Baker. Other solvents and chemicals were used as received. Deionized water was distilled by a water purification system (Milli-Q system). All glassware and Teflon coated magnetic stir bars were cleaned with acetone, followed by copious rinsing with distilled water before drying in an oven at 150 ˚C.

2.2 Characterization methods

Samples for transmission electron microscopy (TEM) and high resolution TEM (HRTEM) analyses were prepared by depositing a single drop of diluted Ni NPs or Ni/SiO_2 catalyst dispersion in hexane or water, respectively, on amorphous carbon coated copper grids. Images were obtained by a JEOL 2010 TEM (200 kV). Powder X-ray diffraction patterns (XRD) were obtained on a Bruker AXS D8 ADVANCE diffractometer with Cu Kα radiation (λ = 1.5418 Å). Elemental analyses of Ni in the samples were carried out using a JY2000 Ultrace inductively coupled plasma atomic emission spectrometer (ICP-AES) equipped with a JY AS 421 autosampler and 2400 g/mm holographic grating after digesting the samples in aqua regia. ^{11}B-NMR spectra were recorded on a Bruker Avance DPX 400 spectrometer with an operating frequency of 128.15 MHz for ^{11}B.

2.3 Synthesis of monodisperse 3.2 nm Ni NPs

Under a nitrogen flow, 257 mg of Ni(acac)$_2$ (1 mmol) was mixed with 15 mL of OAm and 0.32 mL (1 mmol) of OA. The resulting mixture was heated to 110 ˚C over 20 min, resulting in a green solution. The solution was kept at 110 ˚C for 1 h to remove moisture and dissolved oxygen. Next, the solution was cooled down to 90 ˚C whereupon 264 mg of BTB solvated in 2 mL of OAm was quickly injected into the solution. A visible color change from green to dark-brown was observed in less than 1 min. The resulting solution was kept at 90 ˚C for 1 h. The solution was then cooled down to room temperature. The Ni NPs were extracted by addition of 30 mL of ethanol, followed by centrifugation (8500 rpm for 8 min). The product, 3.2 nm Ni NPs, was then dispersed in hexane and kept under a nitrogen atmosphere for the catalytic tests.

2.4 Preparation of 3.2 nm Ni NPs on oxide supports

20 mg of 3.2 nm Ni NPs was dissolved in hexane in a 20 mL vial and mixed with 150 mg of SiO_2 or 100 mg Al_2O_3 or 50 mg CeO_2. These colloidal mixtures were shaken mechanically for 15 h (to ensure complete adherence of Ni NPs to the supports). The resulting catalysts are denoted Ni/SiO_2, Ni/Al_2O_3, and Ni/CeO_2, respectively. The colorless hexane phase was decanted and the solid materials were washed with hexane to remove any unbound Ni NPs. The resulting supported Ni catalysts were redispersed in 10 mL of distilled

water. All catalytic reactions were performed by using these aqueous dispersions of the catalysts.

2.5 Determination of the catalytic activity of oxide-supported 3.2 nm Ni NPs in the hydrolysis of AB

The activity of Ni/SiO_2, Ni/Al_2O_3, and Ni/CeO_2 catalysts in the hydrolysis of AB was determined by measuring the hydrogen generation rate using a typical water-filled gas burette system. Before the activity test, a jacketed reaction flask (25 mL) containing a Teflon coated magnetic stir bar was placed on a magnetic stirrer (VWR International) and thermostated at 25.0 °C ± 1 °C by circulating water through its jacket from a temperature-controlled water bath. Then, a burette filled with water was connected to the reaction flask in order to measure the volume of the hydrogen gas evolved by the reaction. Next, 10 mL of an aqueous dispersion of Ni/support catalyst was transferred into the reaction flask and 128 mg (4 mmol) of AB (corresponding to the generation of a maximum of 12 mmol (267 mL) H_2 gas at 25.0 °C ± 1 °C and 0.91 atm pressure) was added into the catalyst solution which was stirred at 800 rpm. The volume of hydrogen gas evolved was measured by recording the displacement of the water level at intervals of 1 minute.

2.6 Kinetic study of the hydrolysis of AB catalyzed by 3.2 nm Ni/SiO_2

In order to establish the rate law for the hydrolysis of AB catalyzed by 3.2 nm Ni/SiO_2, three different sets of experiments were performed using the basic method described in the previous section. In the first set of experiments, the concentration of AB was kept constant (200 mmol/L) and the nickel concentration was varied (2.5, 4.5, 6.5, and 8.5 mmol/L). In the second set of experiments, the catalyst concentration was fixed at 4.5 mmol/L Ni while the AB concentration was varied (100, 200, 300, 400, and 500 mmol/L). Finally, the catalytic hydrolysis of AB was performed with an AB concentration of 200 mmol/L and 3.2 nm Ni/SiO_2 catalyst concentration of 4.5 mmol/L Ni at various temperatures in the range 20–40 °C in order to obtain an Arrhenius activation energy (E_a). In addition to the volumetric measurement of the hydrogen evolution, the conversion of AB to ammonium metaborate in each experiment was also checked by comparing the relative intensities of the signals due to AB and metaborate anions at δ = –23.9 and 9 ppm, respectively, in the ^{11}B-NMR spectra of the solution.

2.7 Determination of the catalytic activity of 3.2 nm Ni/SiO_2 in the hydrolysis of AB in an inert atmosphere

The hydrolysis of AB catalyzed by Ni/SiO_2 was performed in degassed water in a nitrogen atmosphere. The freeze–pump–thaw cycling method was used for degassing of the water. In a typical freeze–pump–thaw cycling process, a certain amount of water was placed into a Schlenk flask which was sealed. The Schlenk flask was immersed in liquid nitrogen. When the solvent was completely frozen, the flask was opened to the high vacuum and pumped for 10 min, with the flask still immersed in liquid nitrogen. The flask was then closed and warmed until the solvent had completely melted. This process was repeated three times and after the last cycle the flask was backfilled with nitrogen. The activity of the Ni/SiO_2 catalyst in the hydrolysis of AB under the inert atmosphere was determined as described in Section 2.5.

2.8 Determination of the catalytic lifetime of 3.2 nm Ni/SiO_2 in the hydrolysis of AB

The catalytic lifetime of the 3.2 nm Ni/SiO_2 catalyst in the hydrolysis of AB was determined by measuring the total turnover number (TTN). The experiment was carried out using 10 mL of a solution containing 1.0 mmol/L Ni and 500 mmol/L AB at 25 °C ± 1 °C. After conversion of the AB was complete (as shown by stoichiometric H_2 gas evolution (3.0 mol H_2/mol $H_3N{\cdot}BH_3$)), a new batch of 256 mg AB (8 mmol) was added and the completion of the reaction was again established by measuring the H_2 gas evolution. To detect whether ammonia was generated, the gas generated from the catalytic reaction was passed through 25 mL of a standardized solution of 0.001 mol/L HCl at room temperature. After gas generation ceased, the resulting solution was titrated with a standard solution of 0.01 mol/L NaOH by using phenolphthalein as an acid-base indicator. The amount of ammonia released from the reaction can be calculated by comparing the HCl concentrations in the solutions before and after the hydrolysis reaction [23].

3 Results and discussion

3.1 Synthesis of monodisperse 3.2 nm Ni NPs

The monodisperse Ni NPs were formed by the reduction of $Ni(acac)_2$ with BTB in the presence of OAm and OA. In the reaction, OAm acts as both the solvent and a surfactant, BTB serves as the reducing agent, and OA was added as a co-surfactant to stabilize the Ni NPs. The TEM image in Fig. 1(a) shows the 3.2 nm Ni NPs with a standard deviation of ~7% in their size. Figure 1(b) shows a TEM image of a double-layer array of the 3.2 nm Ni NPs from the hexane dispersion and the inset shows the corresponding HRTEM image. The small Ni NPs in the second layer tend to occupy the saddle point between two Ni NPs in the first monolayer assembly, similar to previous observations for small Au, FePt, and PbSe NPs [24, 25]. The presence of OA was found to be the key to obtaining monodisperse Ni NPs because polydisperse Ni NPs with different shape were obtained when OAm alone was used as a surfactant. Optimization experiments to control the Ni NP size by changing the amount of OAm, OA, and BTB showed that 3.2, 4.2, and 5.2 nm Ni NPs could be obtained with molar ratios BTB/Ni of 3, 2, and 1, respectively [22], but there was no direct effect of the amount of OAm and OA on Ni NP size. The larger Ni NPs did not show such narrow size distributions as that for the 3.2 nm size range, indicating that BTB facilitates uniform Ni nucleation and growth. Having observed such an effect of the reducing agent on Ni NP size, we attempted to use the borane–morpholine (BM) complex as a milder reducing agent than BTB to obtain larger Ni NPs, but ca. 3 nm Ni NPs were still obtained. These results indicate that the synthetic conditions employed are especially suitable for making ca. 3 nm Ni NPs.

3.2 Ni NPs supported on oxides as catalysts for the hydrolysis of AB

We recently communicated that Ni NPs supported on amorphous carbon showed good catalytic activity for the hydrolysis of AB [22]. Our further tests indicated that the Ni/C catalyst had very limited stability under the reaction conditions. The low stability may arise from the weak interactions between Ni NPs and the carbon support. If an oxide support is used, then Ni NPs should have a strong interaction with the oxide surface via the formation of interfacial Ni–O bonds, leading to a more robust Ni catalyst for the hydrolysis of AB. Ni/SiO_2, Ni/Al_2O_3, and Ni/CeO_2 with 13, 20, and 40 wt.% Ni, respectively, were employed as catalysts in the hydrolysis of AB without any further treatment being employed to remove the surfactants from the surface of the NPs. Figure 2(a) shows a representative TEM image of the 3.2 nm Ni NPs deposited on a SiO_2 support. Figure 2(b) shows plots of the hydrogen generation versus time from the hydrolysis of AB in the presence 3.2 nm Ni NPs on the different metal oxides. Of the various Ni NP/support catalysts, Ni/SiO_2 gives the highest activity with a TOF value of 13.2 mol

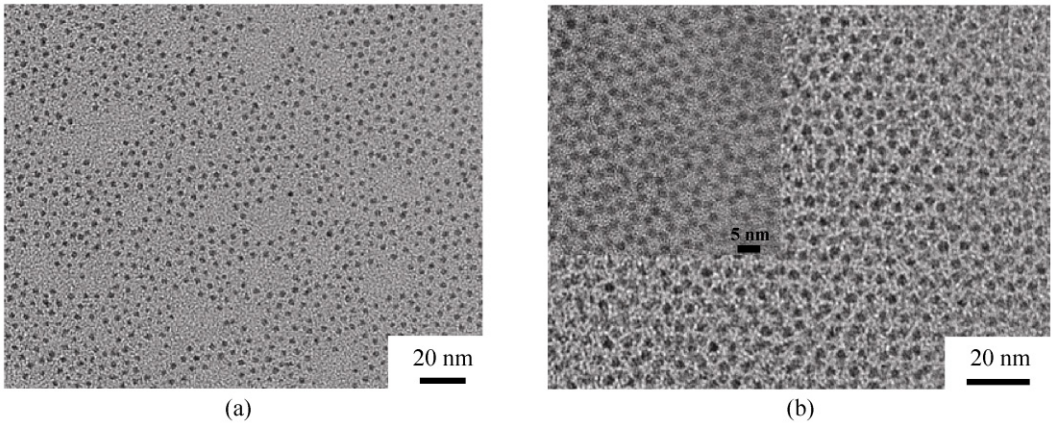

Figure 1 TEM images of (a) the 3.2 nm Ni NPs and (b) the self assembled two-dimensional array of the 3.2 nm Ni NPs. Inset: The two-dimensional array of the Ni NPs at a higher magnification

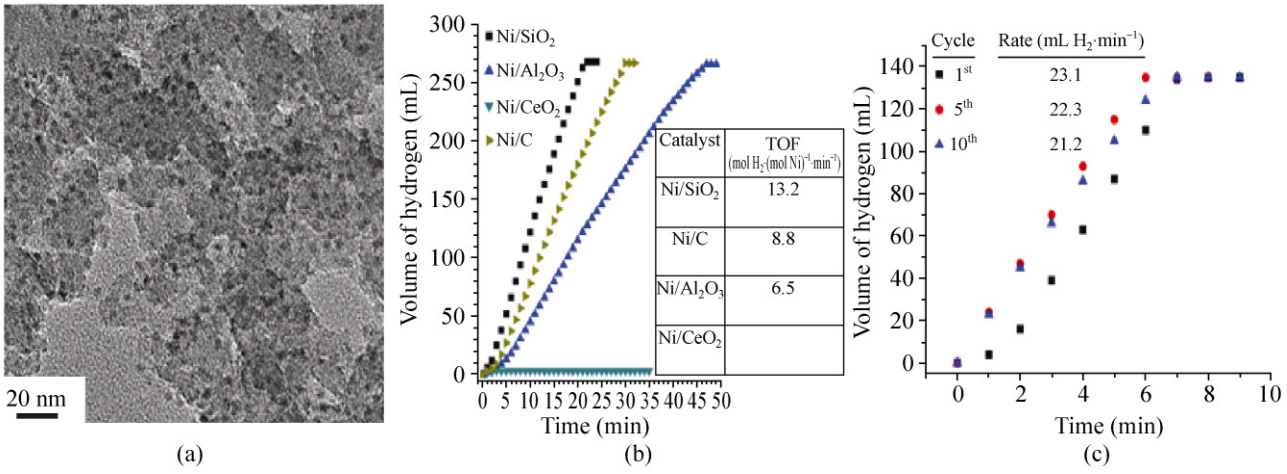

Figure 2 (a) TEM image of the 3.2 nm Ni NPs on a SiO_2 support. (b) Plots of the volume of hydrogen generated versus time in the hydrolysis of AB catalyzed by 3.2 nm Ni NPs on different supports. The inset shows the TOF values for each catalyst. (c) Recyclability tests for the 3.2 nm Ni/SiO_2 catalyst in the hydrolysis of AB. The inset shows the TOF values for hydrogen generation from the hydrolysis of AB catalyzed by Ni/SiO_2 catalyst in different cycles

H_2·(mol Ni)$^{-1}$·min^{-1}, while the Ni NPs in Ni/CeO_2 are deactivated totally (the TOF values were calculated based on the overall Ni content). In addition to its high activity, Ni/SiO_2 is also stable during AB hydrolysis and retains 93% of its initial activity when reused in ten catalytic runs in aqueous solution (Fig. 2(c)). For this reason, the Ni/SiO_2 catalyst was chosen for the further kinetic studies.

To understand the reason behind the enhanced activity and stability of the 3.2 nm Ni/SiO_2 catalyst in the hydrolysis of AB, we took samples of solid catalyst and the reaction solution in different catalytic cycles before the addition of new batch of AB. The solid samples were purified by washing with water and then characterized by TEM, while the solutions were analyzed for Ni content by ICP-AES. Figure 3(a) shows a TEM image of the Ni/SiO_2 catalyst after the 1st cycle. Its morphology is similar to that of the as-synthesized Ni NPs. After the 5th cycle, the TEM image reveals that both 3.2 nm Ni NPs and smaller ~1.6 nm Ni NPs co-exist. The amount of the 1.6 nm Ni NPs increased with the increasing number of catalytic cycles while the amount of the 3.2 nm Ni NPs was correspondingly reduced. After the 10th cycle, only 1.6 nm Ni NPs were present in the NP/SiO_2 sample (Fig. 3(b)). Figure 3(c) shows the change in Ni content in the reaction solution with increasing number of catalytic cycles. It can be seen that the Ni content in the catalytic reaction solution first increases with the number of catalytic cycles. Its content reaches a maximum after the 7th cycle after which the amount of Ni present in the reaction solution is reduced. After the 15th cycle, the Ni content drops back to a level similar to that after the 1st cycle. From these changes in the Ni content of the reaction solutions and the corresponding TEM analyses of the NP/SiO_2 solid samples, we can conclude that the 3.2 nm Ni NPs on SiO_2 are initially subject to reactant etching in the catalytic solution forming Ni(Ⅱ) ions. This etching is likely caused by oxidation of the Ni NPs by oxygen dissolved in the reaction system. However, these Ni(Ⅱ) ions in the solution can be reduced by AB and a new Ni nucleation and growth process occurs under the catalytic reaction conditions, giving 1.6 nm Ni NPs that are deposited directly on SiO_2 support. As a result of this NP re-formation process, the Ni(Ⅱ) concentration measured in the reaction solution after the 7th catalytic cycle drops significantly (Fig. 3(c)). The changes in the Ni NP catalyst as it is repeatedly reused in the hydrolysis of AB are summarized in Fig. 3(d). It should be noted that a control experiment, in which $NiCl_2$ and AB were mixed in aqueous solution, resulted in no hydrogen generation and Ni(Ⅱ) was not reduced to Ni(0). This confirms that the AB hydrolysis is only catalyzed by

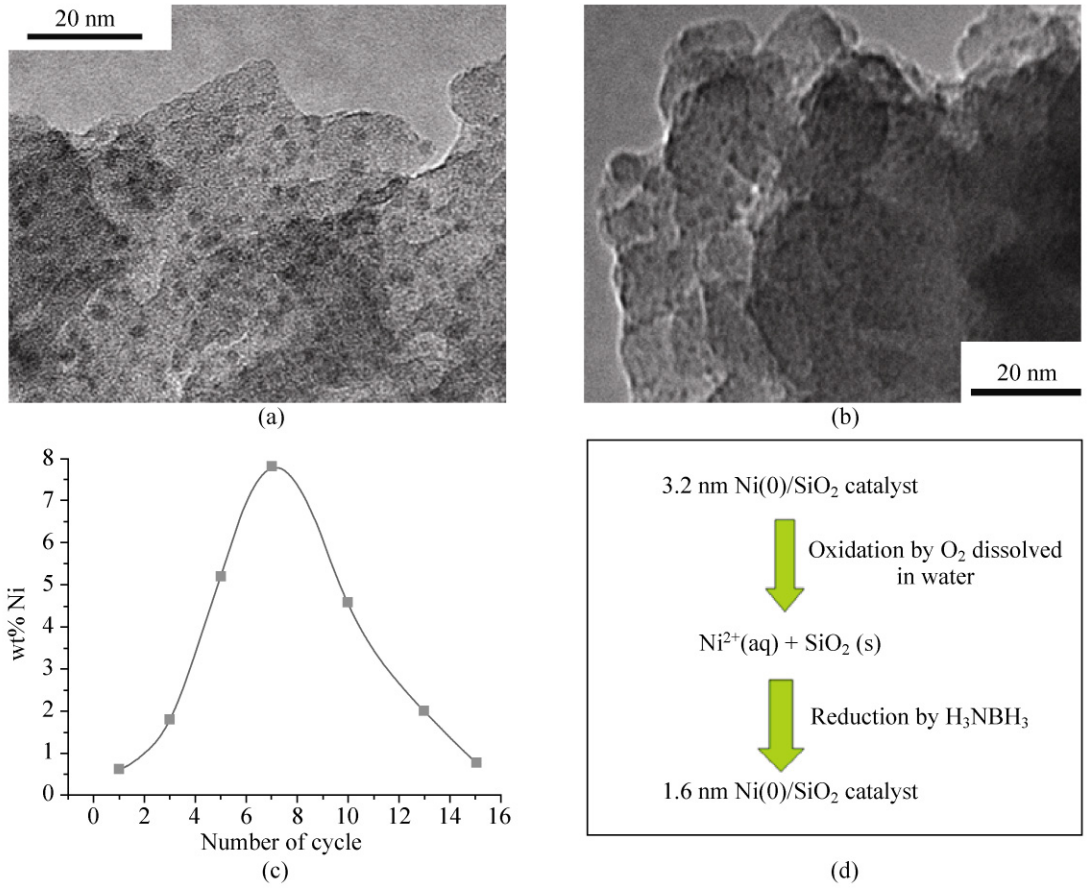

Figure 3 TEM images of the Ni/SiO_2 catalyst in the hydrolysis of AB after (a) the 1st and (b) the 10th catalytic cycle. (c) Plot of wt% Ni released into solution versus number of cycles of hydrolysis of AB catalyzed by Ni/SiO_2. (d) A proposed scheme for the formation of 1.6 nm Ni NPs from the 3.2 nm Ni NPs during the catalytic hydrolysis of AB

Ni NPs, and not by Ni(Ⅱ) ions in the reaction solution.

In a further control experiment involving the hydrolysis of AB catalyzed by Ni/SiO_2 in an inert atmosphere, the Ni/SiO_2 catalyst showed lower catalytic activity than when the reaction was carried out in air, with a TOF of 9.9 mol H_2·(mol Ni)$^{-1}$·min^{-1} (Fig. S-1 in the Electronic Supplementary Material (ESM)). In addition, the TEM image of the catalyst removed from the reaction solution (Fig. S-2 in the ESM). After the first cycle showed only the original Ni NPs with no smaller Ni NPs being observed. These results support the idea that the higher catalytic activity of Ni/SiO_2 in air stems from the formation of 1.6 nm Ni NPs during the hydrolysis of AB.

3.3 Kinetic study of the hydrolysis of AB catalyzed by the 3.2 nm Ni/SiO_2 catalyst

Figure 4 shows plots of the volume of hydrogen generated versus time during the catalytic hydrolysis of 200 mmol/L AB solution in the presence of different Ni concentrations at 25 ℃ ± 1 ℃. The hydrogen generation rate was determined from the linear portion of the plot for each experiment. The inset in Fig. 4 shows the plot of hydrogen generation rate versus concentration of Ni on a logarithmic scale. The slope, 0.98, is very close to unity indicating that hydrolysis of AB catalyzed by 3.2 nm Ni/SiO_2 catalyst is first order with respect to the Ni concentration.

The effect of substrate concentration on hydrogen generation rate was also studied. Figure 5 summarizes the results of a series of experiments performed at 25 ℃ ± 1 ℃ with various initial AB concentrations and a constant catalyst concentration at 4.5 mmol/L Ni. It can be seen that the hydrogen generation from the catalytic hydrolysis of AB shows a half-order dependence on AB concentration. This half-order

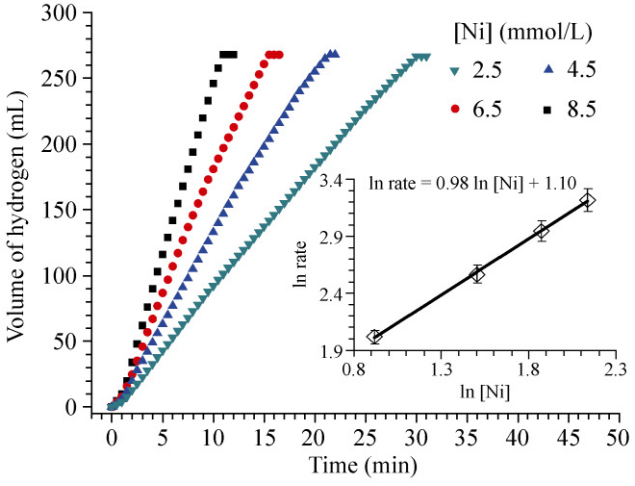

Figure 4 Plots of the volume of hydrogen generated versus time for catalytic hydrolysis of AB with different Ni concentrations ([AB] = 200 mmol/L; T = 25 ˚C ± 1 ˚C). The inset shows the plot of hydrogen generation rate versus the concentration of Ni (both on logarithmic scales)

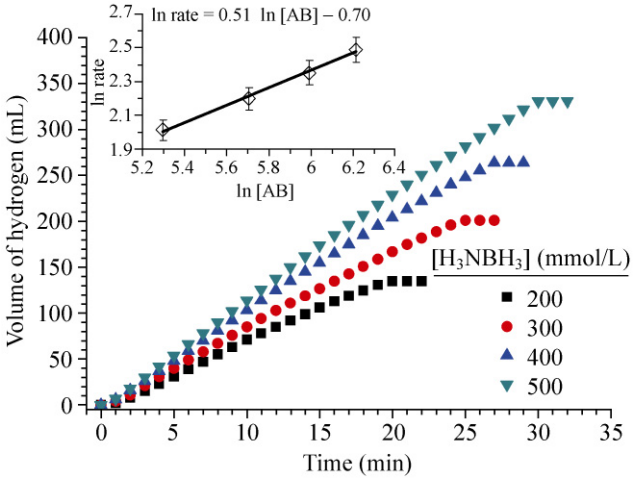

Figure 5 Plots of the volume of hydrogen generated versus time for catalytic hydrolysis of AB with different AB concentrations ([Ni] = 4.5 mmol/L; T = 25 ˚C ± 1 ˚C). The inset shows the plot of hydrogen generation rate versus the concentration of AB (both on logarithmic scales)

dependence on AB concentration is unusual for the catalytic hydrolysis of AB which is generally zero or first order in AB concentration [26, 27]. Interestingly, the same 3.2 nm Ni NPs supported on Ketjen carbon black were found to have zero order kinetics with respect to the AB concentration in the same hydrolysis reaction [22]. Such a half-order dependence on AB concentration may stem from the dissolution of the Ni NP catalyst and reformation of a large number of smaller 1.6 nm Ni NPs on SiO_2 (Fig. 3(d)), resulting in the faster hydrolysis kinetics with SiO_2 as a support than on carbon.

The hydrolysis of AB catalyzed by 3.2 nm Ni/SiO_2 was carried out at various temperatures (20–40 ˚C) in the presence of 200 mmol/L AB and 4.5 mmol/L Ni. The values of the rate constant k at different temperatures were calculated from the slope of the linear region of each plot in Fig. 6 by using the rate law equation.

The activation energy (the Arrhenius plot is shown in the inset of Fig. 6) is calculated to be E_a = 34 kJ/mol ± 2 kJ/mol. This is one of the lowest activation energies reported for the catalytic hydrolysis of AB [28], although the value is 6 kJ/mol higher than that which we previously found for the 3.2 nm Ni/C catalyst [22]. The surface Ni dissolution from Ni NPs supported on SiO_2 and the reformation of Ni NPs on the SiO_2 surface may contribute to the increase in activation energy.

Catalyst lifetime at 25.0 ˚C ± 1 ˚C was measured in terms of TTN, which was found to have a value of 15,400 over 52 h. Ammonia, one of the possible products generated due to incomplete hydrolysis, was also monitored at certain time intervals by using acid/base titrations with a detection limit of ~0.12% by weight [23]. No ammonia was detected in any of the Ni/SiO_2 catalyzed hydrolysis reactions, indicative of complete hydrolysis of the AB complex.

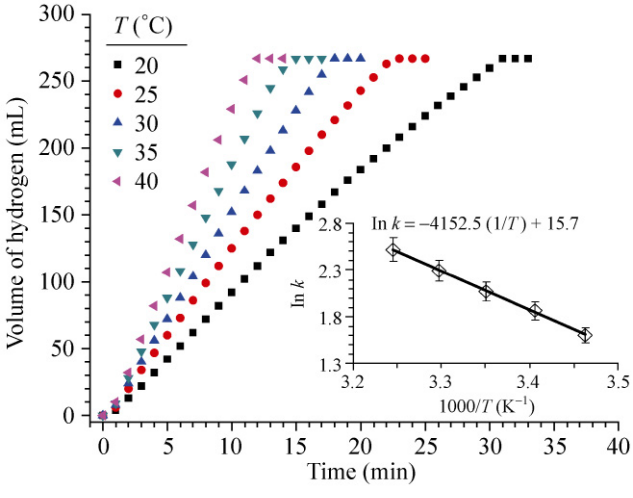

Figure 6 Plots of volume of hydrogen generated versus time for catalytic hydrolysis of AB at different temperatures ([AB] = 200 mmol/L; [Ni] = 4.5 mmol/L). The inset shows the Arrhenius plot (ln k versus the reciprocal absolute temperature $1/T$ K^{-1})

Actually, the absence of ammonia generation during the hydrolysis of AB is not surprising given our reaction conditions, in which the amounts of AB and Ni are smaller than 2 wt% and 0.05 wt%, respectively [23]. Hydrogen generation slows down as the reaction proceeds and ultimately stops due to the increased viscosity of the solution and/or the deactivating effect of metaborate. Much higher TTN values should be possible if the increase in viscosity could be avoided or metaborate could be removed from the reaction system.

4. Conclusions

We have reported detailed studies of the synthesis and characterization of a Ni/SiO_2 catalyst and its catalysis of the hydrolysis of AB. The monodisperse 3.2 nm Ni NPs are prepared by reduction of $Ni(acac)_2$ by BTB in the presence of OAm and OA as stabilizers. Without any special treatment to remove the surfactants, the 3.2 nm Ni NPs supported on SiO_2 are active and durable in the hydrolysis reaction. The high activity and stability of the Ni/SiO_2 catalyst stem from the in situ formation of very small Ni NPs generated from the reduction of Ni(Ⅱ) ions etched into the reaction solution by the partial oxidation of the Ni/SiO_2. Kinetic studies show that the catalytic hydrolysis of AB is first order with respect to the Ni/SiO_2 catalyst concentration but half-order with respect to the AB concentration. The Arrhenius activation energy of the hydrolysis of AB catalyzed by 3.2 nm Ni/SiO_2 is determined to be E_a = 34 kJ/mol ± 2 kJ/mol—one of the lowest activation energies reported for the catalytic hydrolysis of AB. Furthermore, 3.2 nm Ni/SiO_2 is a long-lived catalyst and has a TTN of 15,400 in the hydrolysis reaction. These results indicate that 3.2 nm Ni/SiO_2 is a promising candidate to replace noble metals for the catalysis of AB hydrolysis and for hydrogen generation under ambient conditions.

Acknowledgements

ÖM thanks The Scientific and Technological Research Council of Turkey (TUBITAK) for a 2214-Research Fellowship Program and the METU-DPT-OYP program on the behalf of Atatürk University.

Electronic Supplementary Material: Supplementary material (comparison of the activities of Ni/SiO_2 catalyst in the hydrolysis of AB in air and an inert atmosphere (Fig. S-1 in the ESM), TEM images of the Ni/SiO_2 catalyst after the hydrolysis of AB in an inert atmosphere (Fig. S-2 in the ESM), and plots of volume of hydrogen released versus time for the hydrolysis of AB catalyzed by Ni/SiO_2 in successive catalytic cycles (Fig. S-3 in the ESM)) is available in online version of this article at http://dx.doi.org/10.1007/s12274-010-0031-7 and is accessible free of charge.

References

[1] Schlapbach, L.; Züttel, A. Hydrogen storage materials for mobile applications. *Nature* **2001**, *414*, 353–358.

[2] Orimo, S.; Nakamori, Y.; Eliseo, J. R.; Züttel, A.; Jensen, C. M. Complex hydrides for hydrogen storage. *Chem. Rev.* **2007**, *107*, 4111–4132.

[3] Marder, T. B. Will we soon be fueling our automobiles with ammonia–borane? *Angew. Chem. Int. Ed.* **2007**, *46*, 8116–8118.

[4] Chen, Y. S.; Fulton, J. L.; Linehan, Y. C.; Autrey, T. *In situ* XAFS and NMR study of rhodium-catalyzed dehydrogenation of dimethylamine borane. *J. Am. Chem. Soc.* **2005**, *127*, 3254–3255.

[5] Gutowska, A.; Li, L. Y.; Shin, Y. S.; Wang, C. M.; Li, X. H. S.; Linehan, J. C.; Smith, R. S.; Kay, B. D.; Schmid, B.; Shaw, W.; Gutowski, M.; Autrey, T. Nanoscaffold mediates hydrogen release and the reactivity of ammonia borane. *Angew. Chem. Int. Ed.* **2005**, *44*, 3578–3582.

[6] Stephens, F. H.; Pons, V.; Baker, R. T. Ammonia–borane: The hydrogen source par excellence? *Dalton Trans.* **2007**, 2613–2626, and references therein.

[7] Chandra, M.; Xu, Q. A high-performance hydrogen generation system: Transition metal-catalyzed dissociation and hydrolysis of ammonia–borane. *J. Power Sources* **2006**, *156*, 190–194.

[8] Chandra, M.; Xu, Q. Dissociation and hydrolysis of ammonia–borane with solid acids and carbon dioxide: An efficient hydrogen generation system. *J. Power Sources* **2006**, *159*, 855–860.

[9] Xu, Q.; Chandra, M. Catalytic activities of non-noble metals

for hydrogen generation from aqueous ammonia–borane at room temperature. *J. Power Sources* **2006**, *163*, 364–370.

[10] Kalidindi, S. B.; Sayal, U.; Jagirdar, B. R. Nanostructured Cu and Cu@Cu_2O core shell catalysts for hydrogen generation from ammonia–borane. *Phys. Chem. Chem. Phys.* **2008**, *10*, 5870–5874.

[11] Basu, S.; Brockman, A.; Gagore, P.; Zheng, Y.; Ramachandran, P. V.; Delgass, W. N.; Gore, J. P. Chemical kinetics of Ru-catalyzed ammonia–borane hydrolysis. *J. Power Sources* **2009**, *188*, 238–243.

[12] Yan, J. -M.; Zhang, X. -B.; Han, S.; Shioyama, H.; Xu, Q. Magnetically recyclable Fe–Ni alloy catalyzed dehydrogenation of ammonia borane in aqueous solution under ambient atmosphere. *J. Power Sources* **2009**, *194*, 478–481.

[13] Yan, J. -M.; Zhang, X. -B.; Han, S.; Shioyama, H.; Xu, Q. Room temperature hydrolytic dehydrogenation of ammonia borane catalyzed by Co nanoparticles. *J. Power Sources* **2010**, *195*, 1091–1094.

[14] Cheng, F.; Ma, H.; Li, Y.; Chen, J. $Ni_{1-x}Pt_x$ (x = 0–0.12) hollow spheres as catalysts for hydrogen generation from ammonia borane. *Inorg. Chem.* **2007**, *46*, 788–794.

[15] Clark, T. J.; Whittell, G. R.; Manners, I. Highly efficient colloidal cobalt- and rhodium-catalyzed hydrolysis of $H_3N{\cdot}BH_3$ in air. *Inorg. Chem.* **2007**, *46*, 7522–7527.

[16] Zahmakıran, M.; Özkar, S. Zeolite framework stabilized rhodium(0) nanoclusters catalyst for the hydrolysis of ammonia–borane in air: Outstanding catalytic activity, reusability and lifetime. *Appl. Catal. B: Env.* **2009**, *89*, 104–110.

[17] Chandra, M.; Xu, Q. Room temperature hydrogen generation from aqueous ammonia–borane using noble metal nano-clusters as highly active catalysts. *J. Power Sources* **2007**, *168*, 135–142.

[18] Durap, F.; Zahmakıran, M.; Özkar, S. Water soluble laurate-stabilized ruthenium(0) nanoclusters catalyst for hydrogen generation from the hydrolysis of ammonia–borane: High activity and long lifetime. *Int. J. Hydrogen Energy* **2009**, *34*, 7223–7230.

[19] Yan, J. -M.; Zhang, X. -B.; Han, S.; Shioyama, H.; Xu, Q. Synthesis of longtime water/air-stable Ni nanoparticles and their high catalytic activity for hydrolysis of ammonia–borane for hydrogen generation. *Inorg. Chem.* **2009**, *48*, 7389–7393.

[20] Umegaki, T.; Yan, J. -M.; Zhang, X. -B.; Shioyama, H.; Kuriyama, N.; Xu, Q. Preparation and catalysis of poly(*N*-vinyl-2-pyrrolidone) (PVP) stabilized nickel catalyst for hydrolytic dehydrogenation of ammonia–borane. *Int. J. Hydrogen Energy* **2009**, *34*, 3816–3822.

[21] Jiang, H. -L.; Umegaki, T.; Akita, T.; Zhang, X. -B.; Haruta, M.; Xu, Q. Bimetallic Au–Ni nanoparticles embedded in SiO_2 nanospheres: Synergetic catalysis in hydrolytic dehydrogenation of ammonia borane. *Chem. Eur. J.* **2010**, *16*, 3132–3137.

[22] Metin, Ö.; Mazumder, V.; Özkar, S.; Sun, S. Monodisperse nickel nanoparticles and their catalysis in hydrolytic dehydrogenation of ammonia borane. *J. Am. Chem. Soc.* **2010**, *132,* 1468–1469.

[23] Ramachadran, P. V.; Gagare, P. D. Preparation of ammonia borane in high yield and purity, methanolysis, and regeneration. *Inorg. Chem.* **2007**, *46*, 7810–7817.

[24] Shevchenko, E. V.; Talapin, D. V.; Murray, C. B.; O'Brien, S. Structural characterization of self-assembled multifunctional binary nanoparticle superlattices. *J. Am. Chem. Soc.* **2006**, *128*, 3620–3637.

[25] Kim, J.; Rong, C.; Liu, J. P.; Sun, S. Dispersible ferromagnetic FePt nanoparticles. *Adv. Mater.* **2009**, *21*, 906–909.

[26] Metin, Ö.; Sahin, S.; Özkar, S. Water-soluble poly(4-styrenesulfonic acid-co-maleic acid)-stabilized ruthenium(0) and palladium(0) nanoclusters as highly active catalysts in hydrogen generation from the hydrolysis of ammonia–borane. *Int. J. Hydrogen Energy* **2009**, *34*, 6304–6313.

[27] Metin, Ö.; Özkar, S. Hydrogen generation from the hydrolysis of ammonia–borane and sodium borohydride using water-soluble polymer-stabilized cobalt(0) nanoclusters catalyst. *Energy Fuels* **2009**, *23*, 3517–3526.

[28] Rakap, M.; Ozkar, S. Hydrogen generation from the hydrolysis of ammonia–borane using intrazeolite cobalt(0) nanoclusters catalyst. *Int. J. Hydrogen Energy* **2010**, *35*, 3341–3346.